Effect of metastable Mg_2Si and dislocations on α-Al(MnFe)Si dispersoid formation in Al-Mn-Mg 3xxx alloys

Zhen Li, Zhan Zhang, X.-Grant Chen *

Department of Applied Science, University of Quebec at Chicoutimi,
Saguenay, QC, Canada, G7H 2B1

Abstract

The effect of metastable Mg_2Si and dislocations on the formation of α-Al(MnFe)Si dispersoids in Al-Mn-Mg 3xxx alloys were studied by a close examination of the dispersoid precipitation process using the quench technique and TEM observation. Special attention was paid to the nucleation mechanisms. Mg plays an important role in promoting the formation of α-Al(MnFe)Si dispersoids. The number density and volume fraction of the dispersoids in the Mg containing alloy are much higher than those in the control alloy without Mg, resulting in a strong dispersoid strengthening effect. During the heating process in the Mg containing alloy, metastable Mg_2Si precipitated and dissolved, leaving local Si-rich areas on pervious metastable Mg_2Si, which provide favorable nucleation sites for α-Al(MnFe)Si dispersoids. It was found that β'-Mg_2Si precipitates were more effective at the promotion of the dispersoid nucleation than β''-Mg_2Si. In the deformed sample, the dislocations become the preferable sites for the α-Al(MnFe)Si dispersoid nucleation. By reducing dispersoid free zones, the dispersoid distribution became more uniform compared to the non-deformed sample. The dispersoid nucleation mechanisms based on both metastable Mg_2Si and dislocations are proposed and discussed.

Keywords: Al-Mn-Mg 3xxx alloys; Dispersoid precipitation; Nucleation mechanism; Microstructure; TEM observation

* Corresponding author – X.-Gant Chen, Tel: (418) 545-5011 ext. 2603; Fax: (418) 545-5012;
Email: xgrant.chen@uqac.ca

1. Introduction

Traditional Al-Mn-Mg 3xxx alloys are widely used for architecture, packaging and automobile applications due to their excellent corrosion resistance, formability and weldability. Though 3xxx alloys are normally classified as non-heat-treatable alloys, a strong dispersoid strengthening effect has been discovered in recent years by applying a suitable heat treatment [1-5]. Formed during heat treatment, α-Al(MnFe)Si dispersoids are the key strengthening phase in the aluminum matrix, which greatly improves the strength of 3xxx alloys, particularly at elevated temperature [6]. α-Al(MnFe)Si dispersoids have a partial coherence with the aluminum matrix [4, 7] and are thermally stable up to 573 K (300 °C) [1, 3, 8], which leads 3xxx alloys to be promising candidates for elevated temperature applications .

During heating process of the heat-treatment, metastable Mg_2Si could precipitate in some Al-Mn-Mg-Si alloys because of the presence of Mg and Si. The precipitation sequence of Mg_2Si in Mg and Si containing aluminum alloys was generally described as follows: Mg and Si clusters → needle-like β″-Mg_2Si → lath-like or rod-like β′-Mg_2Si → plate-like equilibrium β-Mg_2Si [9-14]. The typical size of the needle-like β″-Mg_2Si precipitates is in the range of 4 x 4 x 50 nm [11]. The lath-like or rod-like β′-Mg_2Si precipitates have dimensions of approximately 10 x 10 x 500 nm [12]. The size of the plate-like equilibrium β-Mg_2Si phase can reach to several micrometers [9, 15, 16]. It was reported in previous studies [17-20] that metastable Mg_2Si precipitates could have a positive effect on the nucleation of α-Al(MnFeCr)Si and α-AlMnSi dispersoids in 6xxx alloys. It was observed during the dispersoid formation [18] that there existed an intermediate phase, the u-phase, that first nucleated on the β′-Mg_2Si and that the α-Al(MnFeCr)Si dispersoids heterogeneously nucleated on these ‘u-phase’ precipitates. However, the effect of metastable Mg_2Si on the nucleation of Mn-containing dispersoids has not been systematically investigated.

It is well known that some defects, such as vacancies and dislocations, may enhance the precipitation kinetics of the secondary precipitation phase due to the increasing number of nucleation sites and diffusivities of the alloying elements in the materials [21-26]. There were a few reports that documented the precipitation behavior of dispersoids in deformed 3xxx alloys [27, 28], in which the plastic deformation increased the number density and volume fraction of the dispersoids. This could be attributed to the increase of nucleation sites and diffusion rate by dislocations. It is worth mentioning that the above reported alloys did not contain Mg, and thus,

no Mg_2Si existed. This suggests that the dislocations in the deformed samples could have an impact on dispersoid nucleation in addition to the possible Mg_2Si nucleation effect.

In our previous work [29], the effects of Mg and Si on α-Al(MnFe)Si dispersoid precipitation, elevated-temperature strength and creep resistance in 3xxx alloys were systematically studied, in which there was an evidence that pre-existing $\beta^{'}$-Mg_2Si could promote the formation of α-Al(MnFe)Si dispersoids. The aim of the present work is to clarify the effects of metastable Mg_2Si and dislocations on the nucleation and growth of α-Al(MnFe)Si dispersoids in the Al-Mn-Mg 3xxx alloys. The influence of metastable Mg_2Si on the nucleation of the dispersoids was investigated by a close examination of the dispersoid precipitation process using the quench technique and TEM observation. The effect of different types of metastable Mg_2Si on the dispersoid formation was also evaluated using two-step heat treatments. Moreover, the effect of dislocations on the nucleation of dispersoids in the deformed samples was studied and compared to the non-deformed control sample.

2. Experimental procedures

Two experimental Al-Mn-Mg 3xxx alloys were used in this study. The base alloy, used as a control material, contains 1.25%Mn, 0.25%Si and 0.6%Fe (all of the alloy compositions are in wt% unless indicated otherwise). The main alloy investigated contains additionally 1%Mg, while the concentrations of Mn, Si and Fe remain the same as in the base alloy. The two alloys were prepared from commercially pure Al (99.7%), and Mg (99.9%), and Al-25%Mn, Al-25%Fe and Al-50%Si master alloys. The chemical compositions of the experimental alloys were analyzed using an optical emission spectrometer and are listed in Table 1. In each test, approximately 3 kg of material was prepared in a clay-graphite crucible using an electric resistance furnace. The temperature of the alloy melt was maintained at 1032 K (750 °C) and then degassed for 15 minutes. The melt was then poured into a pre-heated permanent steel mold. The dimension of the cast ingot is 30 x 40 x 80 mm.

Table 1 Chemical composition of experimental alloys (wt%)

Alloy code	Si	Fe	Mn	Mg	Al
Base	0.23	0.56	1.23	**0.002**	Bal.
M1	0.26	0.57	1.25	**1.00**	Bal.

To examine the influence of metastable Mg_2Si and dislocations on the dispersoid nucleation, the as-cast or deformed samples were heat-treated under different heat treatment procedures. In procedure A, the samples were heated with a constant heating rate of 5 K/min in an electrical resistance furnace from room temperature to the desired temperature. Samples were heated to either 548 K (275 °C) or 648 K (375 °C), or in some cases held at 648 K (375 °C) for various holding times, followed by water quench to room temperature. A schematic diagram of the heat treatment is shown in Fig. 1a. Procedure B is the two-step heat treatment, in which the samples were directly put in the furnace at 448 K (175 ºC) for 5 hours and 523 K (250 ºC) for 12 hours respectively, followed by water quench to room temperature. Then, the samples were put into a furnace directly at 648 K (375 ºC) and held for 24 hours followed by water quench (see Fig. 1b).

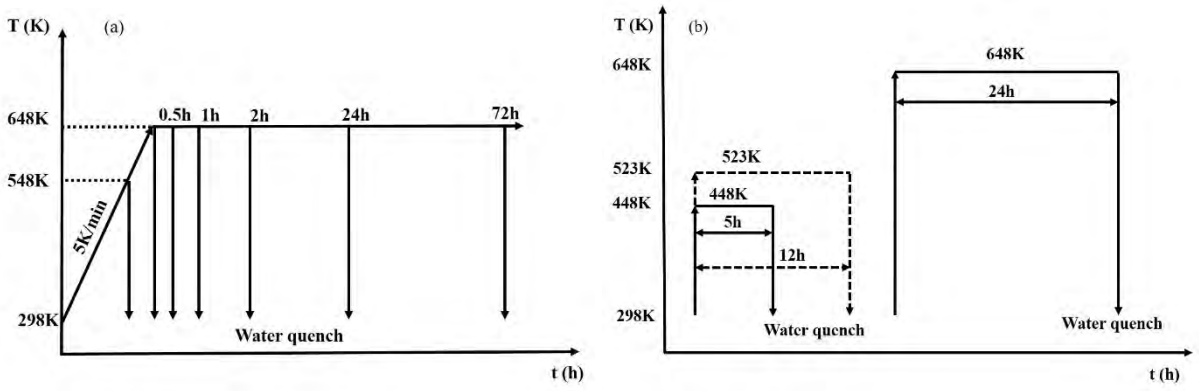

Fig. 1 Schematic diagram of various heat treatments (a) procedure A and (b) procedure B (two-step heat treatment).

For the deformation test, the samples were machined to a cylindrical form with 15 mm in length and 10 mm in diameter. In the tests, the samples were cold-compressed to 0.2 true strain at a strain rate of 10^{-3} s^{-1} on a Gleeble 3800 thermomechanical testing machine.

After heat treatment, the samples were prepared using the conventional metallographic method. The polished samples were etched by 0.5%HF for 20 seconds to reveal the dispersoids. An optical microscope equipped with an imaging analysis system (Clemex PE 4.0) was used to observe the distribution of the dispersoids and to quantify the dispersoid free zone (DFZ). Vicker

hardness was measured by an NG-1000 CCD microhardness test machine with a load of 200 g and a dwell time of 20 s. A transmission electron microscope (TEM, JEM-2100) equipped with an energy dispersive X-ray spectroscopy (EDS) was used to observe the dispersoids in details. TEM foils were prepared in a twin jet electropolisher using a solution of 30% nitric acid in methanol at -20 ºC. To evaluate of the dispersoid volume fraction, the thicknesses of TEM foils were measured using the electron energy loss spectroscopy (EELS) equipped on the TEM. The size and number density of the dispersoids were measured by using imaging analysis (Clemex PE 4.0) on the TEM images. The volume fraction of dispersoids, *Vv*, was calculated using Eq. 1 [6].

$$V_v = A_A \frac{K\bar{D}}{K\bar{D} + t}(1 - A_{DFZ}) \quad (1)$$

where A_A is the area percentage of dispersoids measured with TEM images and $\bar{D}$ is the average equivalent diameter of dispersoids from the TEM images; t is the TEM foil thickness; A_{DFZ} is the area percentage of dispersoid free zone; and K is the shape factor of dispersoids and its value of 0.45 was taken from [6], in which the morphology of dispersoids in AA3xxx alloys was similar to the morphology of dispersoids in the present work.

3. Results and discussion

3.1 Precipitation of α-Al(MnFe)Si dispersoids in the base alloy

Fig. 2 shows the typical microstructure of the base alloy (Mg-free) after heat treatment at 648 K (375 °C) for 24 h and at 648 K (375 °C) for 72 h. The large needle-like and plate-like particles are Al_6(Mn,Fe) intermetallics, which originate from the as-cast microstructure and are distributed in interdendrite regions. The small black dots are α-Al(MnFe)Si dispersoids, which precipitated during the heat treatment and were revealed after etching with 0.5% HF. The Al_6(Mn,Fe) and α-Al(MnFe)Si phases were identified in the previous work [1]. After heat-treatment at 648 K (375 °C) for 24 h, only a few of the dispersoids appeared around intermetallic particles, which left an extensive dispersoid free zone (DFZ) in the microstructure, as shown in Fig. 2a. With a prolonged heat treatment up to 72 h (Fig. 2b), more dispersoids precipitated out of the matrix. However, the amount of dispersoids precipitated is still limited. The area fraction of DFZ after 648 K (375 °C) for 24 h reached as high as 79%, while the area fraction of DFZ after 648 K (375 °C) for 72 h still remained at 51.4%. Fig. 3 shows the TEM bright field images, which dispays the dispersoids in details. The α-Al(MnFe)Si dispersoids have cubic-like or rod-

like morphologies with a composition close to $Al_{12\text{-}20}(MnFe)_3Si$. In the sample treated 648 K (375 °C) for 24 h (Fig. 3a), the number density of the dispersoids was very low and the size was quite large (~97 nm in diameter). After a longer, 72 h treatment (Fig. 3b), the number density of the dispersoids moderately increased and the size slightly decreased to 80 nm. The volume fraction of dispersoids after 648 K (375 °C) for 24 h was only 0.32% and it increased to 0.82% after 648 K (375 °C) for 72 h. After solidification, there was a supersaturated solid solution of Mn and Si in the aluminum matrix, which tended to decompose for dispersoid precipitation during heat treatment. Results indicate that the precipitation of α-Al(MnFe)Si dispersoids in the base alloy was very difficult. After 24 h at 648 K (375 °C), only a small amount of dispersoids (0.32%) precipitated, and the amount was still limited even after a prolonged 72 h treatment.

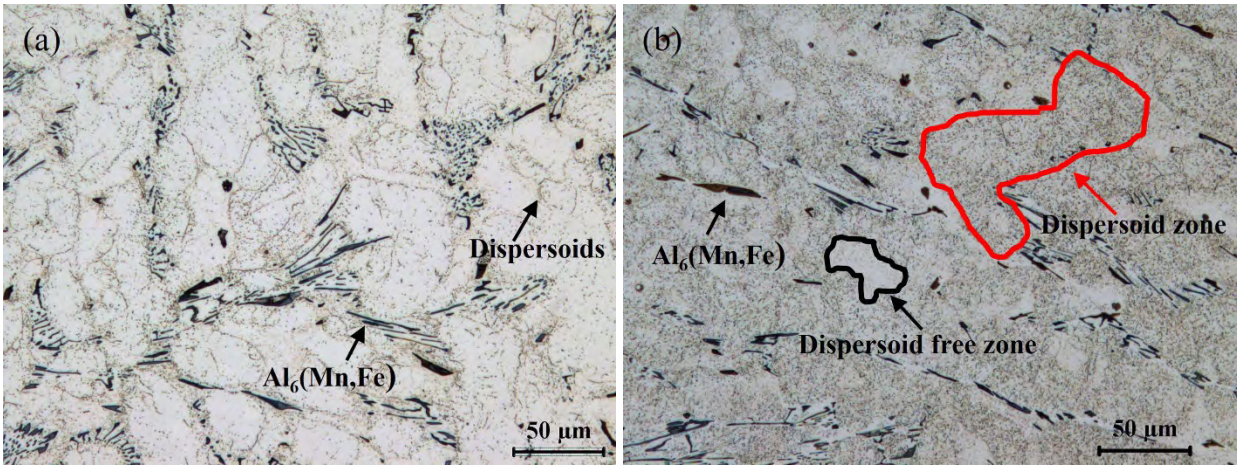

Fig. 2 Optical images showing the dispersoid distribution in the base alloy, (a) 648 K (375 °C) for 24 h and (b) 648 K (375 °C) for 72 h.

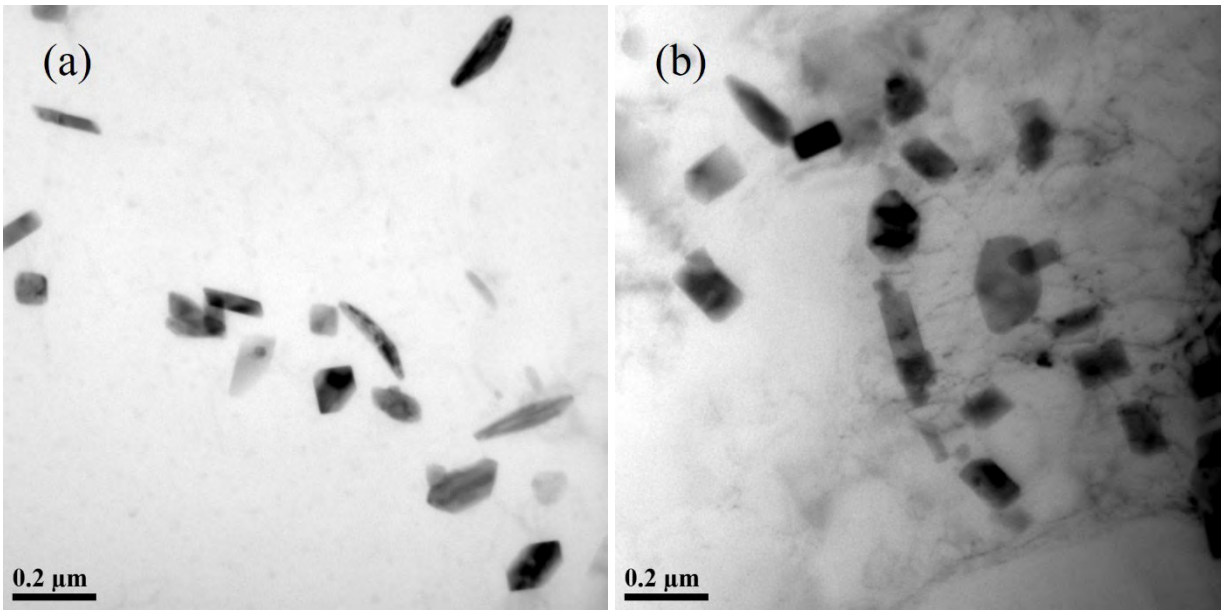

Fig. 3 TEM bright field images showing the dispersoids in the base alloy, (a) 648 K (375 °C) for 24 h and (b) 648 K (375 °C) for 72 h, recorded near $[001]_{Al}$ zone axis.

3.2 Precipitation of α-Al(MnFe)Si dispersoids in the M1 alloy

The precipitation of α-Al(MnFe)Si dispersoids in the Mg containing alloy (M1) after 648 K (375 °C) for 24 h is shown in Fig. 4a. The dispersoid zone and dispersoid free zone (DFZ) were clearly distinguishable in the optical microstructure after etching, as shown in Fig. 4. The dispersoid zones were centered inside aluminum cells and grains, while the DFZs were located in the interdendrite regions close to the Mn-containing intermetallic particles. With the addition of 1% Mg, a large number of the dispersoids appeared in the microstructure after heat treatment and the precipitation of dispersoids became much easier when compared to the Mg-free base alloy under the same heat treatment condition. The area fraction of the DFZ decreased from 79% in the base alloy to 26.5% in the M1 alloy. TEM observations (Fig. 5a) confirmed that a large number of rod-like or plate-like dispersoids precipitated in the dispersoid zone. The number density and volume fraction of the dispersoids in the M1 alloy were much higher than in the base alloy. It is evident that the presence of Mg greatly promoted the formation of dispersoids.

The typical microstructure of the M1 alloy after the two-step heat treatments (448K(175ºC)/5h + 648K(375ºC)/24h and 523K(250ºC)/12h + 648K(375ºC)/24h) are shown in Fig. 4b and c, respectively. Compared to the 448K(175ºC)/5h + 648K(375ºC)/24h treatment, the

sample that underwent the 523K(250ºC)/12h + 648K(375ºC)/24h treatment showed an increased amount of dispersoids and an reduced DFZ. TEM images (Fig. 5b and c) clearly revealed that the number density of dispersoids in the 448K(175ºC)/5h + 648K(375ºC)/24h sample was smaller than the one step sample (Fig. 5a), and the number density of dispersoids in the 523K(250ºC)/12h + 648K(375ºC)/24h sample increased. All measured results are shown in Table 2. The results show that the area fraction of the DFZ decreases from 30% (448K(175ºC)/5h + 648K(375ºC)/24h) to 23% (523K(250ºC)/12h + 648K(375ºC)/24h). On the other hand, the volume fraction of dispersoids increases from 1.93% (448K(175ºC)/5h + 648K(375ºC)/24h) to 2.15% (523K(250ºC)/12h + 648K(375ºC)/24h). It is apparent that the 448K(175ºC)/5h + 648K(375ºC)/24h treatment is less efficient at promoting the dispersoid precipitation than the 523K(250ºC)/12h + 648K(375ºC)/24h treatment. It was reported that during the heating process both metastable β˝-Mg_2Si and β΄-Mg_2Si could precipitate in alloys containing Mg and Si depending on the heating rate [11, 12]. To obtain the controllable β˝-Mg_2Si or β΄-Mg_2Si precipitation in the samples, the two-step heat treatments with the first step at 448K(175ºC)/5h for β˝-Mg_2Si and at 523K(250ºC)/12h for β΄-Mg_2Si were designed and conducted in the present work. The effect of variants of the metastable Mg_2Si precipitates on the formation of dispersoids and their mechanisms will be discussed later. It is worth to mention that the samples with holding at 448K (175 ºC) and particularly at 523K (250 ºC) for 12 h can reduce the supersaturated Mn solutes in the aluminum matrix. Therefore, it is expected the volume fraction of the dispersoids formed in the two-step treatments is moderately lower than that in the one step treatment.

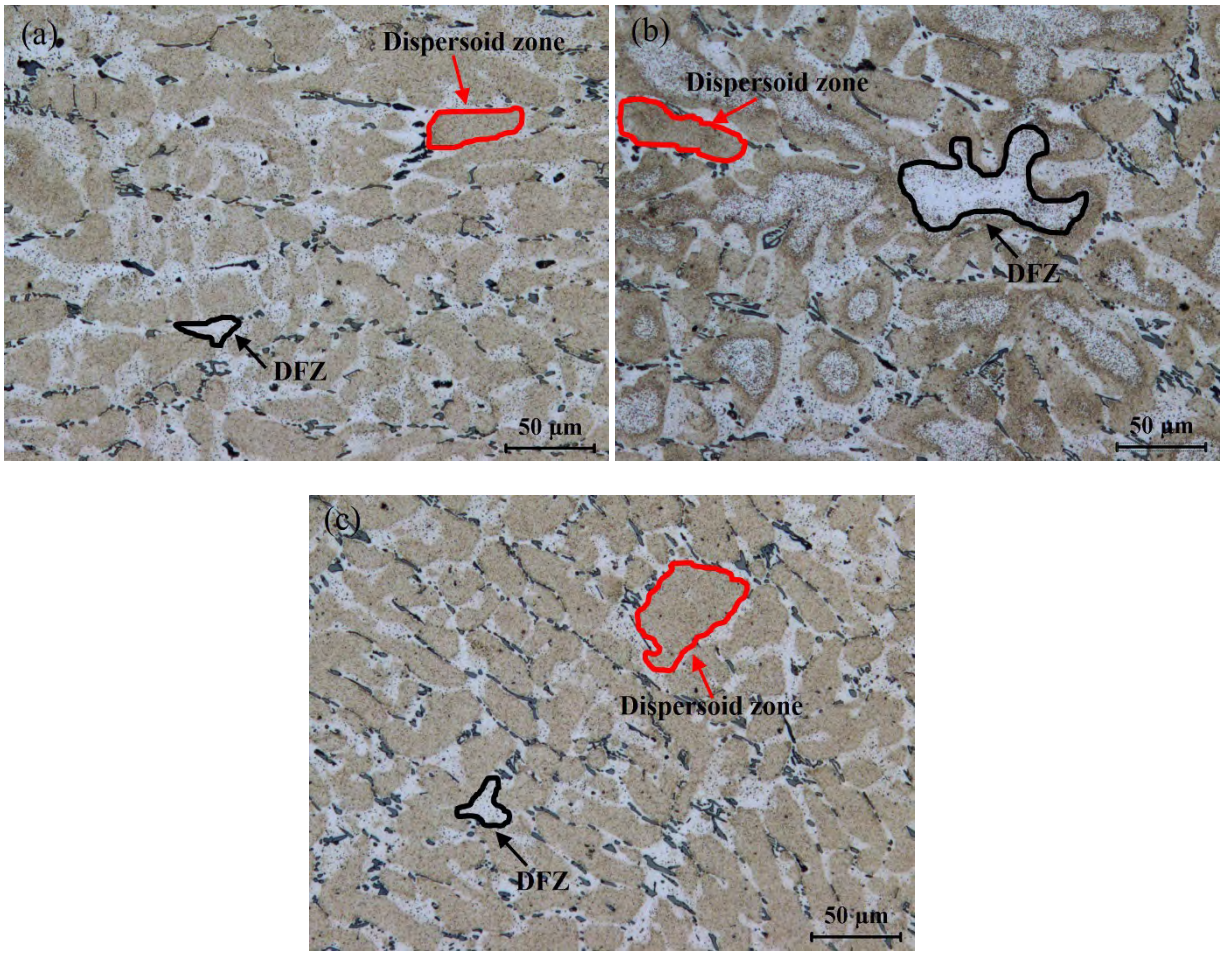

Fig. 4 Optical images showing the precipitation of dispersoids in the M1 alloy under different heat treatment conditions, (a) 648K(375ºC)/24h, (b) 448K(175ºC)/5h + 648K(375ºC)/24h and (c) 523K(250ºC)/12h + 648K(375ºC)/24h.

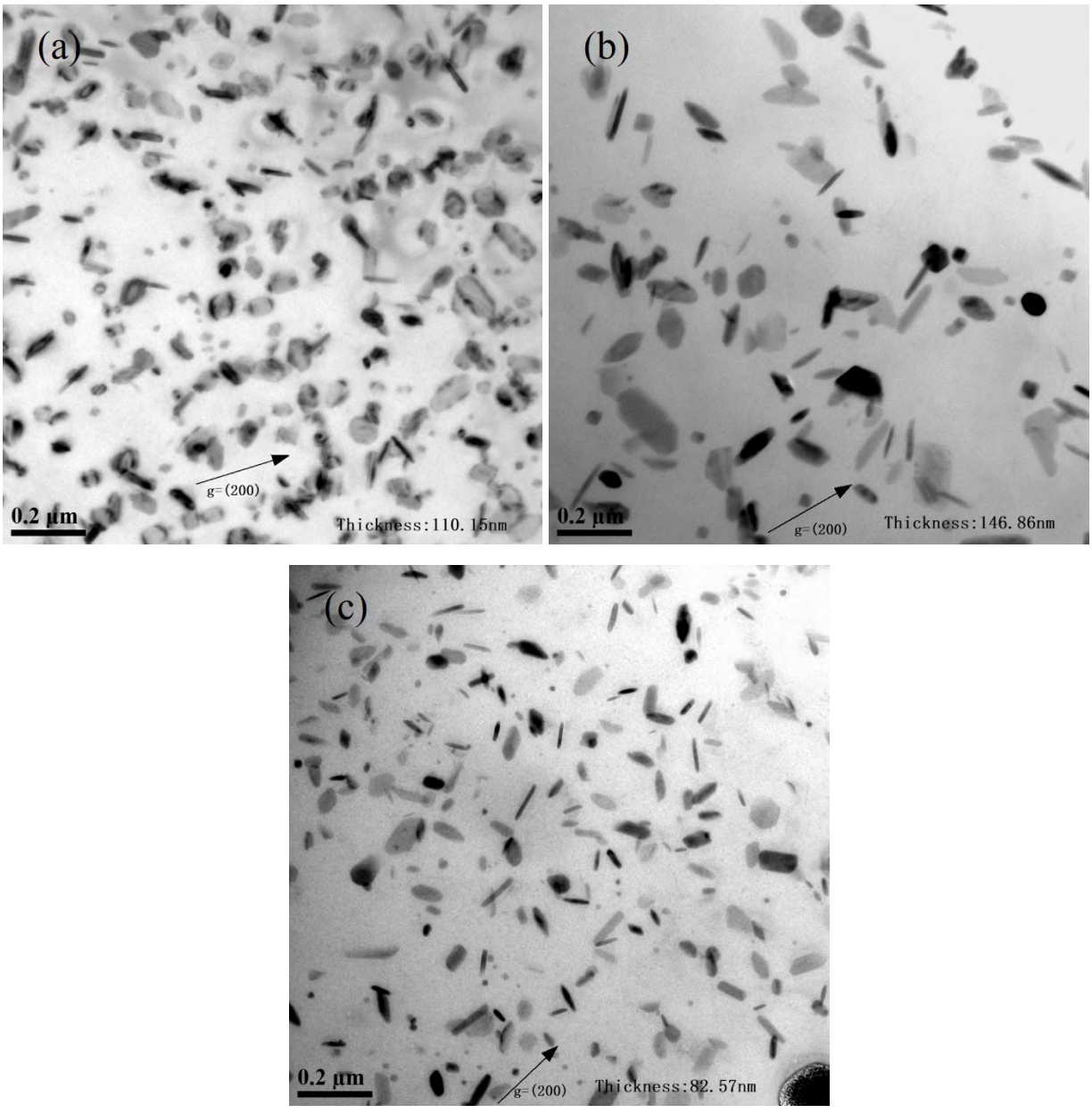

Fig. 5 TEM bright field images showing the dispersoids in the M1 alloy after different heat treatments, (a) 648K(375ºC)/24h, (b) 448K(175ºC)/5h + 648K(375ºC)/24h and (c) 523K(250ºC)/12h + 648K(375ºC)/24h, recorded near the $[001]_{Al}$ zone axis. The arrows indicate the $<100>_{Al}$ orientation.

Table 2 Dispersoid and DFZ parameters measured under different conditions

Alloy	Heat treatment	Area fraction of DFZ (%)	Equivalent diameter of dispersoids (nm)	Number density of dispersoids (μm^{-3})	Volume fraction of dispersoids (%)
Base	648K(375ºC)/24h	79	97	72	0.32
Base	648K(375ºC)/24h	51.4	80	-	0.82
M1 Alloy	648K(375ºC)/24h	26.4	50	1055	2.69
M1 Alloy	448K(175ºC)/5h + 648K(375ºC)/24h	30	56	563	1.93
M1 Alloy	523K(250ºC)/12h + 648K(375ºC)/24h	23	42	1326	2.15
Deformed M1 Alloy	648K(375ºC)/24h	7	68	294	2.58

3.3 Precipitation of α-Al(MnFe)Si dispersoids in the deformed M1 alloy

The optical microstructure of the deformed M1 sample after the heat treatment at 648K(375ºC)/24h is shown in Fig. 6. At first glance, it appears that the dispersoids appeared almost everywhere, and their distribution was more uniform than that of the non-formed M1 alloy (Fig. 4a). Furthermore, hardly any DFZs were observed in the deformed samples. The image analysis results show that the area fraction of DFZ in the deformed samples was only 7.0%, while it was 26.5% in the non-formed M1 alloy (Table 2). This implies that the deformation has a strong benefit on the uniformity of the dispersoid distribution, particularly in the interdendrite regions.

A close observation revealed that the distribution of dispersoids was not uniform in the matrix, and some areas had a higher density than others. To better assess the number density and volume fraction of dispersoids in the deformed sample, the dispersoid zone was further divided to the dense dispersoid zone and the less dense dispersoid zone, as shown in Fig. 6. The former is mostly in the core of the aluminum grain and the latter is found toward the interdendrite region and close to Mn-containing intermetallic particles. TEM observation confirmed the existence of the two different zones and Fig. 7 shows TEM images of the different densities of the α-

Al(MnFe)Si dispersoids in these two zones. To quantify the number density and volume fraction of the dispersoids, the following equations were used in the image analysis on TEM images:

$$N_{av} = N_d \cdot V_d + N_l \cdot V_l \qquad (2)$$

$$V_d = V_{dd} \cdot V_d + V_{dl} \cdot V_l \qquad (3)$$

Where N_{av} is the average number density. N_d and N_l are the number density of dispersoids in the dense dispersoid zone and less dense dispersoid zone, respectively. N_d and N_l were measured by image analysis based on TEM images, which were taken in the zones with high number density of dispersoids and low number density of dispersoids, respectively. V_d and V_l are the volume fractions of the dense dispersoid zone and less dense dispersoid zone, respectively. V_d and V_l were measured by image analysis on the optical images of etched samples. V_{dd} and V_{dl} are the volume fractions of dispersoids in the dense dispersoid zone and less dense dispersoid zone, respectively, which were calculated according to Eq. 1.

The results are listed in Table 2. It can be seen that the dispersoid size is larger and the number density is smaller than it is in the non-deformed sample under the same heat treatment condition. However, the dispersoid volume fraction in the deformed sample is almost the same as that in the non-deformed sample. It was reported that dislocations may enhance the precipitation kinetics of second phase precipitation [21-26]. The effect of deformation and thus the generated dislocations on the dispersoid precipitation will be discussed later.

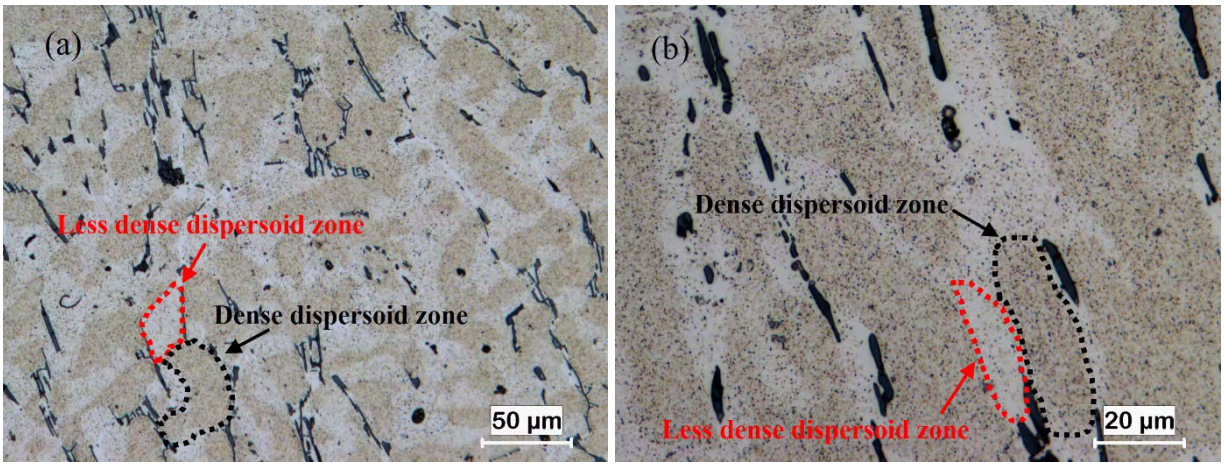

Fig. 6 Optical image showing the precipitation of dispersoids in the deformed M1 alloy after heat treatment at 648K(375ºC)/24h: (a) the dense dispersoid zone and the less dense dispersoid zone and (b) enlarged image of (a).

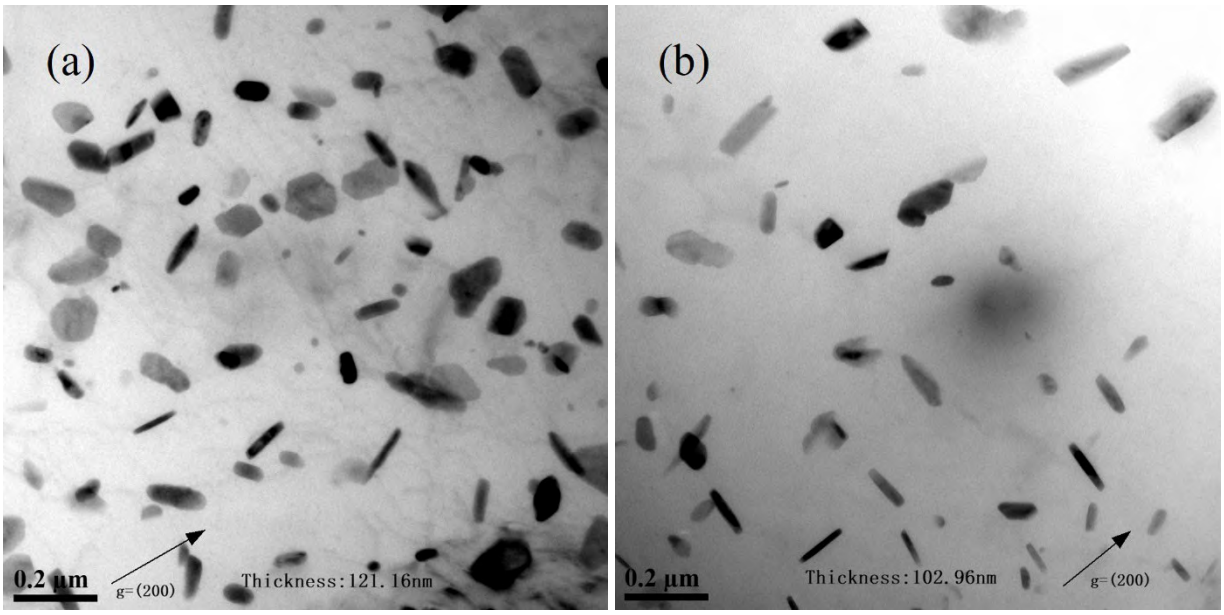

Fig. 7 TEM bright field images showing the dispersoids in the deformed M1 alloy (0.2 strain + 648K(375ºC)/24h), a) in the dense dispersoid zone and b) in the less dense dispersoid zone.

3.4 The effect of Mg and deformation on microhardness

To confirm the dispersiod precipitation and its strengthening effect, the Vicker microhardness of the base and M1 alloys under different conditions was measured. The results of hardness measurements for the base and M1 alloys are shown in Fig. 8. Compared to the base alloy, the hardness values of the Mg containing M1 alloy under all heat treatment conditions are remarkably higher. Those hardness increases include the Mg solid solution strengthening and the dispersoid strengthening. Because no Mg-containing phase is formed after the final heat treatment at 648 K (375ºC) (Figs. 5 and 7), most of Mg solute atoms remain in the aluminum matrix of the M1 alloy. It is reported in our previous work [2] that 1% Mg in solid solution can increase 12-13 MPa of the yield strength in aluminum alloys. Using the relationship YS ≈ HV/3 [30], it represents approximately 4 HV hardness increment. It is apparent that the hardness increases of the Mg containing M1 alloy after the heat treatment is mainly due to the dispersoid strengthening. For example, at the same heat treatment condition (648K(375ºC)/24h), the hardness of the Mg containing M1 alloy is 26 HV higher than that of the base alloy, indicating the strong dispersoid strengthening effect caused by adding Mg.

The hardness of the sample after the 523K(250ºC)/12h + 648K(375ºC)/24h two-step treatment is 65 HV while it is 58 HV for the sample that experienced the 448K(175ºC)/5h + 648K(375ºC)/24h two-step treatment, suggesting that the two-step treatment at 523K(250ºC)/12h + 648K(375ºC)/24h is more effective at enabling the dispersoid strengthening effect, which was confirmed by the optical and TEM observations (Figs. 4 and 5).

The hardness of the deformed sample (0.2 strain compression) is moderately higher than that of the non-deformed M1 sample under the same heat treatment condition. It is worth to mention that the work hardening by the 0.2 strain compression deformation is almost negligible after the heat treatment at 648 K (375ºC). The deformed sample's hardness is similar to the sample after the 523K(250ºC)/12h + 648K(375ºC)/24h two-step treatment. Therefore, the best strengths of materials are achieved by the two-step 523K(250ºC)/12h + 648K(375ºC)/24h treatment and by the deformation.

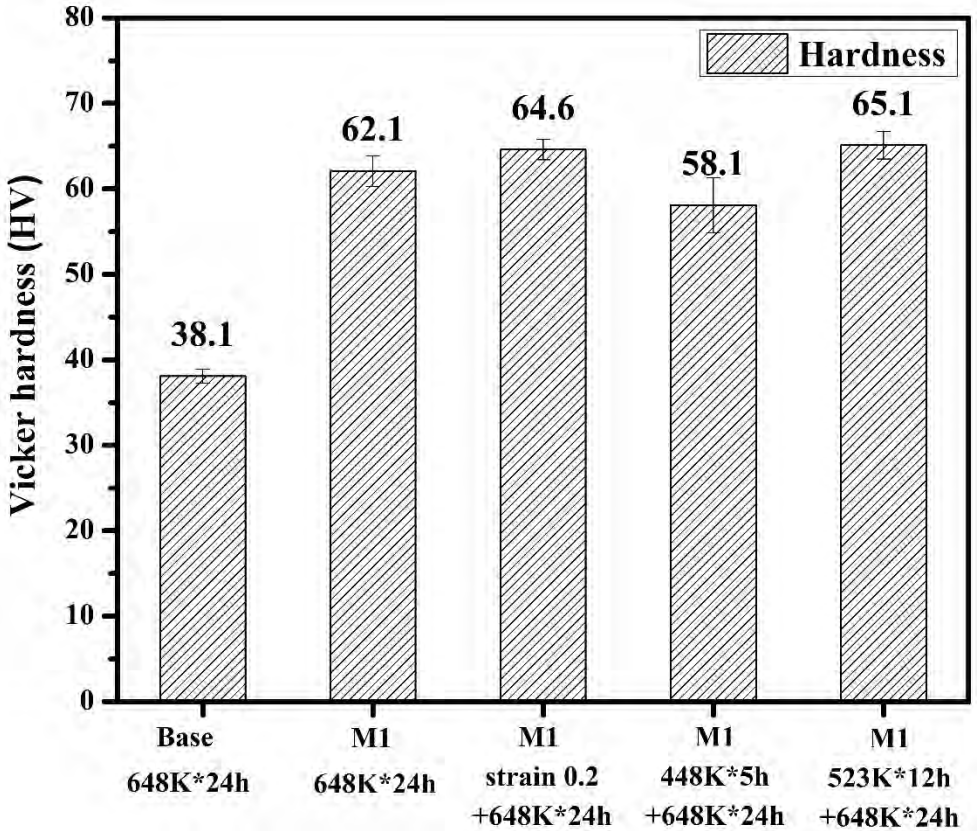

Fig. 8 Microhardness of the base alloy and M1 alloy under various experimental conditions.

3.5 Metastable Mg_2Si-based nucleation mechanism

According to above observation, the number density and the volume fraction of α-Al(MnFe)Si dispersoids in the M1 alloy (1%Mg) are much higher than those in the base alloy without Mg. It should be noted that α-Al(MnFe)Si dispersoids do not contain Mg, which means that Mg is not a necessary component of the α-Al(MnFe)Si phase. The only possible phase containing Mg in the M1 alloy is the metastable Mg_2Si precipitates that appeared during heating process. To explore how Mg and metastable Mg_2Si promote the dispersoid formation, the precipitation process in the M1 alloy during heat treatment was investigated using the quenching technique described in Fig. 1a and TEM analysis.

Fig. 9 shows TEM images of the precipitation of the metastable Mg_2Si precipitates and α-Al(MnFe)Si dispersoids during different stages of the heat treatment. When the samples were heated to 548 K (275 ^{o}C), a number of lath-like precipitates appeared (Fig. 9a), which were identified to be β'-Mg_2Si based on the morphology and orientation of the precipitates [9-12] and the corresponding selected area diffraction pattern (SADP, Fig. 9f) [31]. The small black dots are the cross sections of the lath-like precipitates. These lath-like precipitates growing along $<100>_{Al}$ are approximately 10 nm in width and 100-200 nm in length. It is evident that the supersaturated solid solution after solidification in the M1 alloy was decomposed during the heating to 548 K (275 ^{o}C) and the β'-Mg_2Si precipitated. It should be mentioned that no α-Al(MnFe)Si dispersoids formed at this stage.

After the samples heated to 648 K (375 ^{o}C), all lath-like β'-Mg_2Si dissolved and left only a few of the cubic-like equilibrium Mg_2Si particles (Fig. 9b). No visible α-Al(MnFe)Si dispersoids were observed. During isothermal holding at 648 K (375 ^{o}C), fine α-Al(MnFe)Si dispersoids appeared, and after 30 mins the size of dispersoids was approximately 10-20 nm (Fig. 9c). The dispersoids were distributed along $<001>_{Al}$ direction which is the preferred precipitation orientation of previous β'-Mg_2Si.

After holding for 1 and 2 hours at 648 K (375 ^{o}C), the dispersoids gradually grew, as shown in Figs. 9d and e. The precipitation direction of dispersoids along $<001>_{Al}$ is still clearly visible, which means that most dispersoids nucleated and grew on the previous β'-Mg_2Si sites, even though they dissolved. As the holding time prolonged towards 24 hours, Ostwald ripening (coarsening) occurred and the size of dispersoids after 24 h reached 50 nm, as shown in Fig. 6a and Table 2. Due to a great number of dispersoids, the preferred precipitation direction of the

dispersoids seems to be a little unclear. However, a majority of the dispersoids can still be seen distributed along <001>$_{Al}$ direction. Certainly, after the initial nucleation and growth, the dispersoids might have chances to nucleate and grow on other sites, such as at dislocations. After being heat-treated for 24 h, it is not necessary that all the dispersoids were along <001>$_{Al}$ direction. It is also worth mentioning that the nucleation of the dispersoids on equilibrium β-Mg_2Si was not observed.

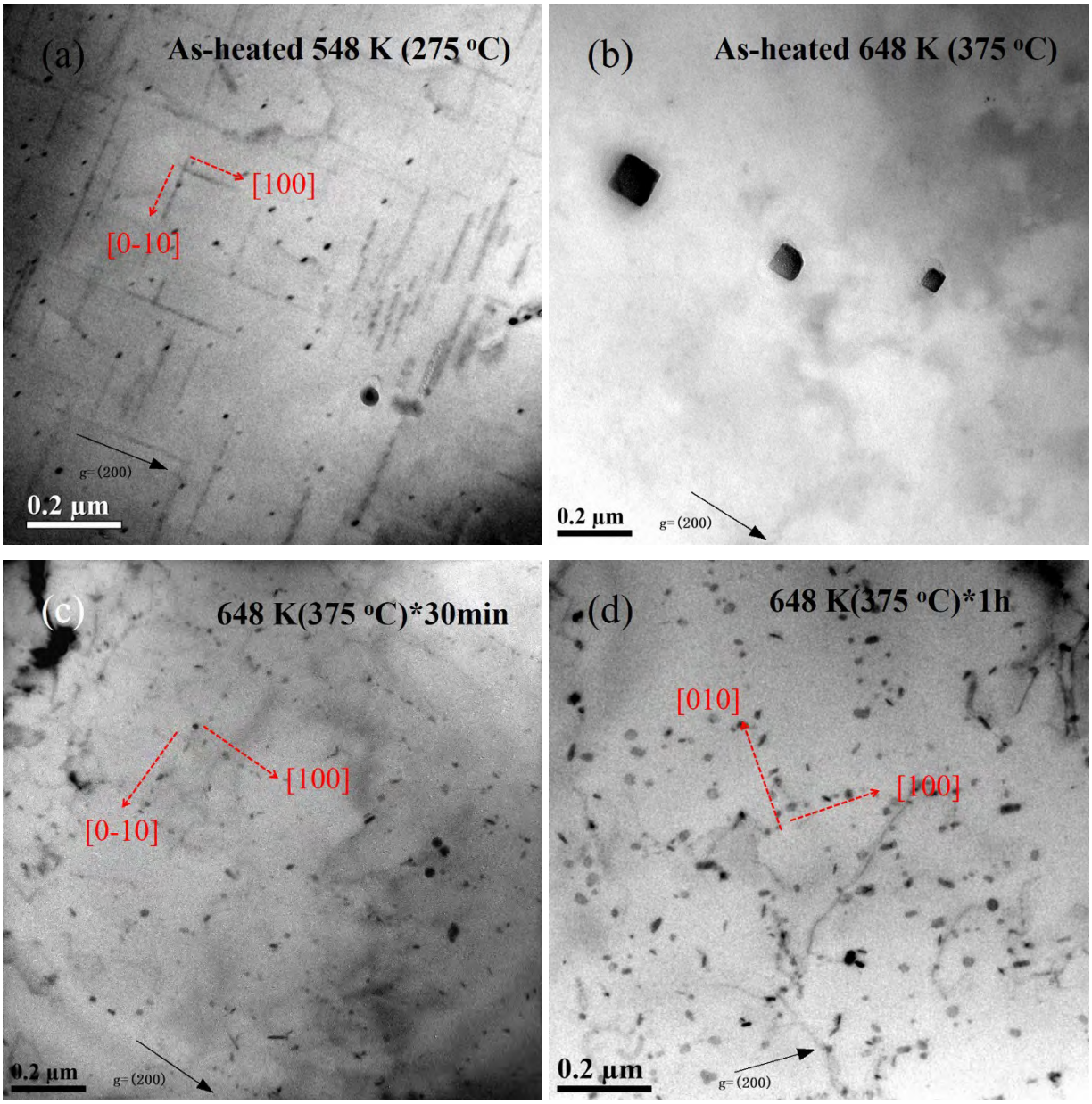

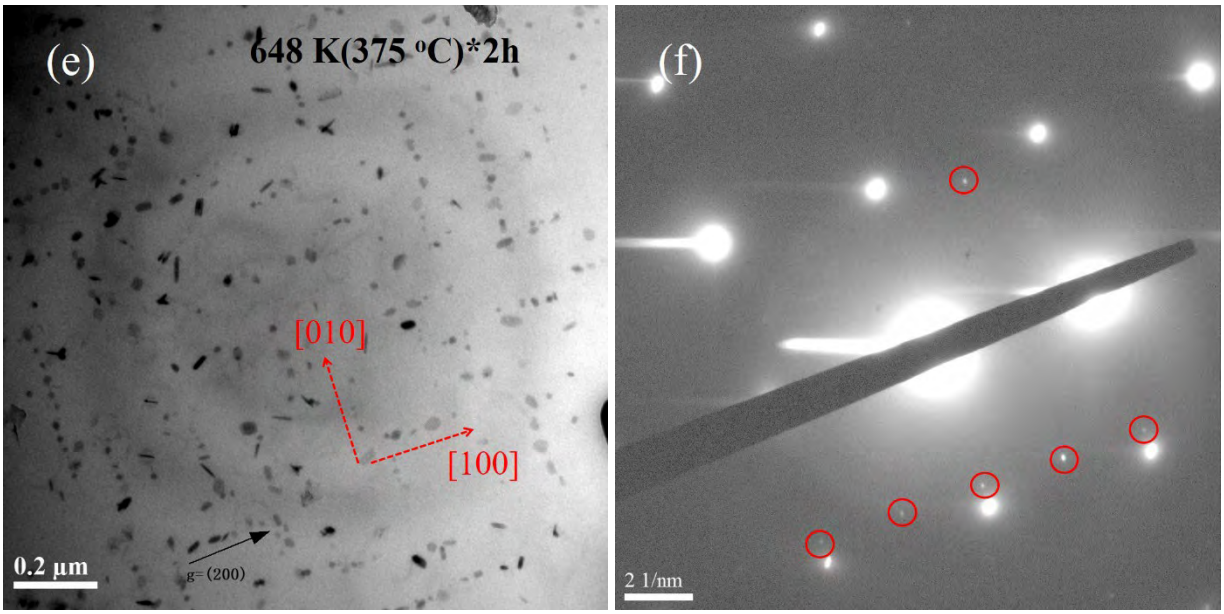

Fig. 9 The precipitation process in the M1 alloy (a) as-heated at 548 K (275 ºC), (b) as-heated at 648 K (375 ºC), (c) 648 K (375 ºC) for 30 min, (d) 648 K (375 ºC) for 1 h, (e) 648 K (375 ºC) for 2 h, (f) the selected area diffraction pattern (SADP) corresponding to the image (a) and the typical diffraction spots of β'-Mg_2Si indicated by the red circles.

The local chemical composition at the sites of dissolved β'-Mg_2Si was analyzed using TEM-EDS line scanning. The typical result of the Si distribution along the dissolved β'-Mg_2Si in the sample held for 15 minutes at 648 K (375 ºC) are shown in Figure 10. It can be seen that a few small α-Al(MnFe)Si particles began to precipitate along $<001>_{Al}$ direction (see Fig. 10a), which was a previous site of β'-Mg_2Si. Across this site (the scan line A-C), the Si concentration at the location of the dissolved β'-Mg_2Si was higher than in the surrounding aluminum matrix (local Si enrichment), as shown in Fig. 10b. As mentioned above, Mg is not a necessary element but Si is the essential element for α-Al(MnFe)Si dispersoid formation. Without Si, α-Al(MnFe)Si dispersoids can hardly form in the matrix. It becomes evident that α-Al(MnFe)Si would preferentially nucleate on the sites of previous β'-Mg_2Si precipitates, which could provide more Si atoms than at other places in the aluminum matrix. It should be noted that the intermediate phase, the u-phase, that could promote the nucleation of α-Al(MnFe)Si reported in [18], has not been observed in the present study, which could be due to the different alloy compositions and heat treatment conditions.

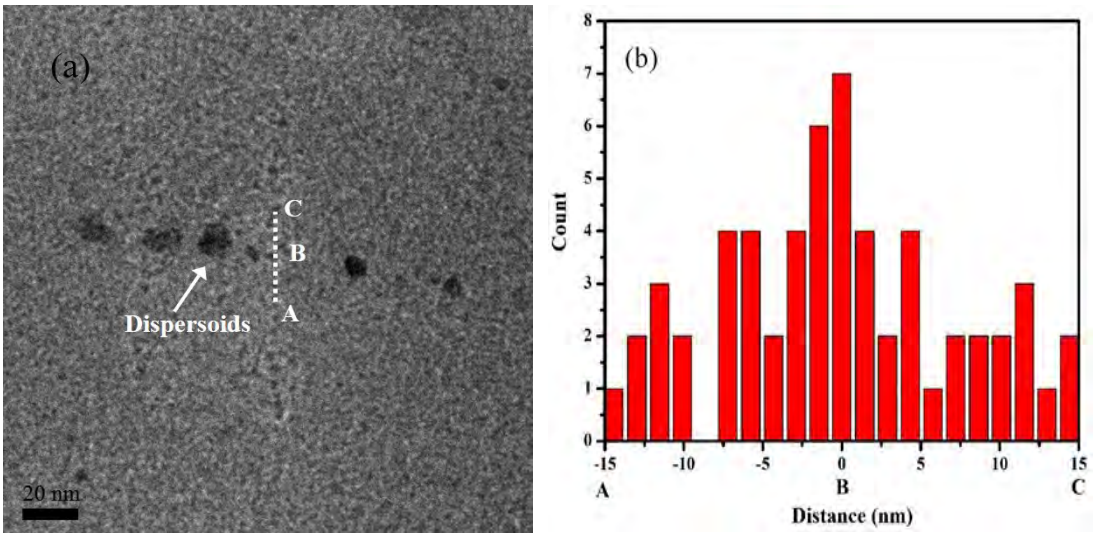

Fig. 10 TEM analysis of the M1 sample held at 648 K (375 ºC) for 15 minutes showing the local Si enrichment on the sites of previous β'-Mg_2Si precipitates, (a) TEM image on the site of a previous β'-Mg_2Si and the position of the line scanning (A-C) and (b) Si distribution along the line A-C.

To further distinguish the effect of the pre-existing β"-Mg_2Si and β'-Mg_2Si on the dispersoid formation, the two-step heat treatments with the first step at 448K(175ºC)/5h and at 523K(250ºC)/12h for controllable β"-Mg_2Si and β'-Mg_2Si were conducted. In the section 3.2, the effect of these two-step heat treatments on the precipitation of α-Al(MnFe)Si dispersoids were described and compared. The details of the precipitation process under these two conditions are shown in Fig. 11. For the sample treated at 448 K (175 ºC) for 5 h, the only phase that appeared was the needle-like β"-Mg_2Si located along the $<001>_{Al}$ direction (Fig. 11a), identified based on the morphology and orientation of the precipitates and the corresponding selected area diffraction pattern (SADP, Fig. 11e) [32]. The needle-like β"-Mg_2Si precipitates were approximately 3 nm in width and 20-100 nm in length. During further heating to 648 K (375 ºC), all needle-like β"-Mg_2Si dissolved in the aluminum matrix. For the sample treated at 523 K (250 ºC for 12 h), the precipitated phase was lath-like β'-Mg_2Si with a size of approximately 10 nm in width and 100-200 nm in length (Fig. 11b), which also dissolved in aluminum matrix during further heating to 648 K (375 ºC). The β'-Mg_2Si was identified based on the corresponding

SADP (Fig. 11f) [31]. After holding for 1 h at 648 K (375 ºC) in both 448K(175ºC)/5h and 523K(250ºC)/12h samples, all of the α-Al(MnFe)Si dispersoids lay along <001>$_{Al}$ direction (Figs. 11c and d), which indicates that the α-Al(MnFe)Si dispersoids nucleated and grew in the sites of previous β˝-Mg_2Si or β΄-Mg_2Si precipitates. Although the β˝-Mg_2Si precipitates in the 448K(175ºC)/5h sample are denser than the β΄-Mg_2Si precipitates in the 523K(250ºC)/12h sample, the amount of α-Al(MnFe)Si dispersoids in the 448K(175ºC)/5h + 648K(375ºC)/1h sample (Fig. 11c) is much lower than that in the 523K(250ºC)/12h + 648K(375ºC)/1h sample (Fig. 11d). Compared to the one step heat treatment sample (648K(375ºC)/1h, Fig. 9d), the amount of α-Al(MnFe)Si dispersoids in the 448K(175ºC)/5h + 648K(375 ºC)/1h sample is also lower. In addition, the number density and volume fraction of the dispersoids in the final treated sample (448K(175ºC)/5h + 648K(375ºC)/24h) are lower than that in the 523K(250ºC)/12h + 648K(375ºC)/24h final sample (Table 2). Here, it has to remind that the number density and volume fraction of the dispersoids in the M1 sample after 448K(175ºC)/5h + 648K(375ºC)/24h treatment is still higher than that in the base alloy without any pre-existing Mg_2Si, showing a positive effect in promoting the dispersoid formation. It is apparent that pre-existing β΄-Mg_2Si precipitates are more effective at promoting dispersoid nucleation than pre-existing β˝-Mg_2Si precipitates. It is most likely that the local Si enrichment of dissolved β΄-Mg_2Si is larger than that of the β˝-Mg_2Si precipitates, because of the large size of β΄-Mg_2Si. This, in turn, creates a more favorable condition for α-Al(MnFe)Si dispersoid nucleation and growth. During the heating process towards higher temperature (648 K (375 ºC)), most of β″- and β′-Mg_2Si dissolved in the aluminum matrix and it left very few equilibrium β-Mg_2Si particles (Fig. 11c). When the precipitation of dispersoids started, it was not observed that the dispersoids nucleated on equilibrium β-Mg_2Si particles.

405

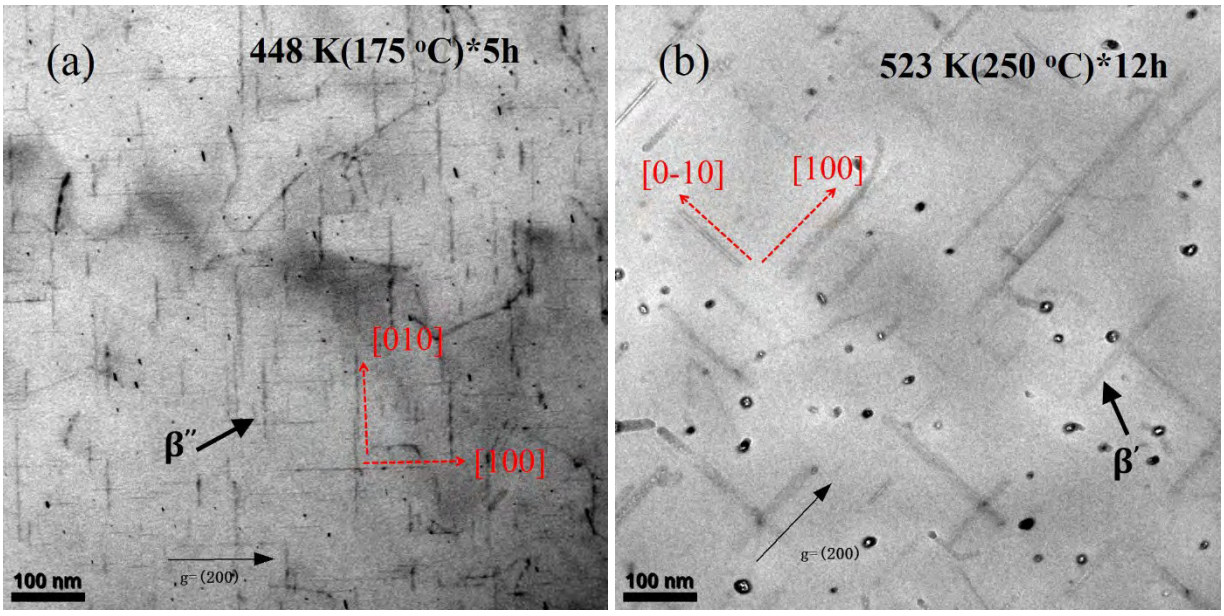
(a)
448 K(175 °C)*5h
[010]
[100]
β″
g=(200)
100 nm
(b)
523 K(250 °C)*12h
[0-10]
[100]
β′
g=(200)
100 nm

406

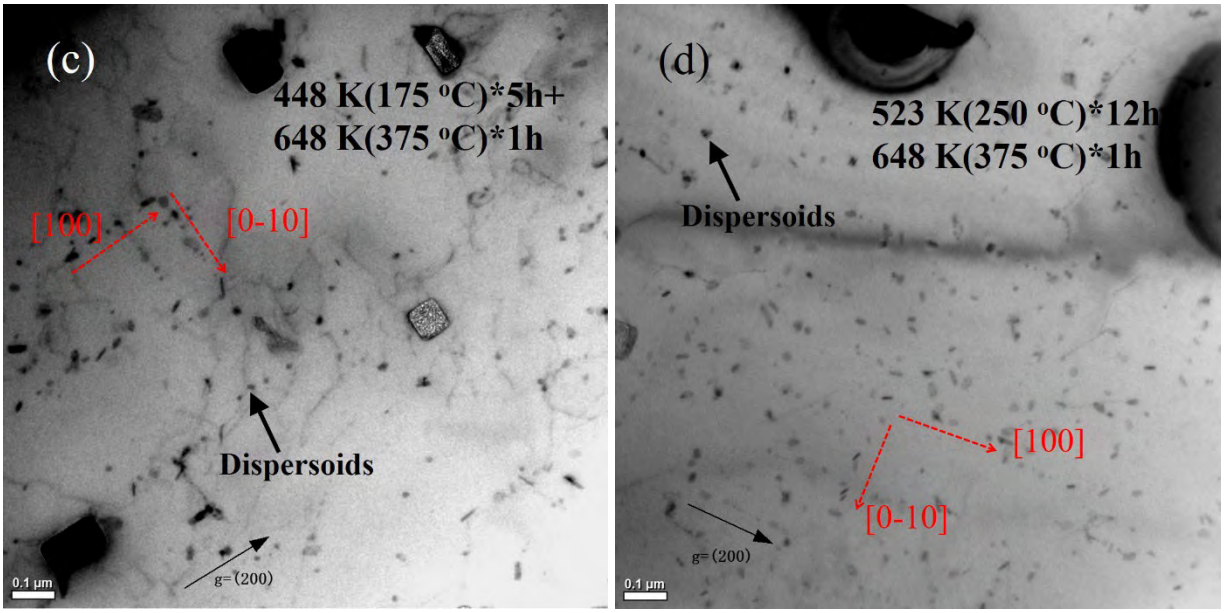
(c)
448 K(175 °C)*5h+
648 K(375 °C)*1h
[100]
[0-10]
Dispersoids
g=(200)
0.1 μm
(d)
523 K(250 °C)*12h
648 K(375 °C)*1h
Dispersoids
[100]
[0-10]
g=(200)
0.1 μm

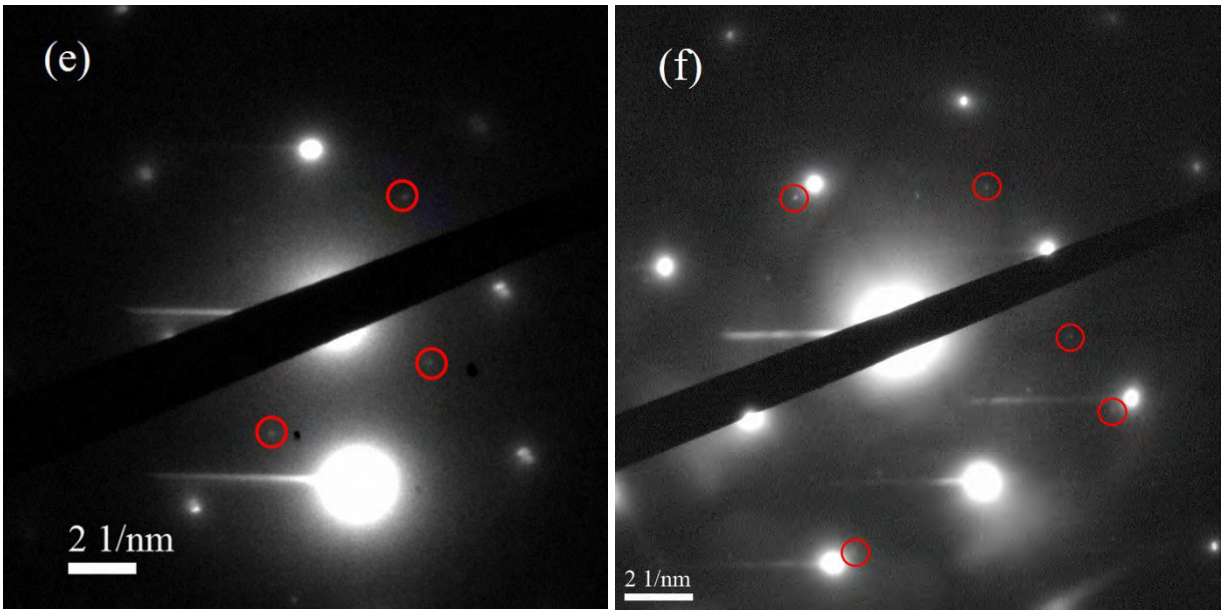

Fig. 11 TEM images of the M1 samples experienced (a) 448 K (175 ºC) for 5 h, (b) 523 K (250 ºC) for 12 h, (c) 448 K (175 ºC) for 5 h + 648 K (375 ºC) for 1 h, (d) 523 K (250 ºC) for 12 h + 648 K (375 ºC) for 1 h, (e) the selected area diffraction pattern (SADP) corresponding to the image (a) and the typical diffraction spots of β″- Mg2Si indicated by the red circles, (f) the selected area diffraction pattern (SADP) corresponding to the image (b) and the typical diffraction spots of β′-Mg_2Si indicated by the red circles.

Based on the above results, the nucleation mechanism of the dispersoids based on the metastable Mg_2Si precipitates can be described as follows (Fig. 12). In the Mg containing M1 samples under various heat treatments (including both one step and two-step treatments), a large number of metastable Mg_2Si phase first precipitated during heating process at the temperature range of 423-548 K (150-275 ºC) (Fig. 12a), and then gradually dissolved at higher temperatures of 573-648 K (300-375 ºC) (Fig. 12b). The sites of the dissolved metastable Mg_2Si were still Si-rich, which provided favorable sites for the nucleation of α-Al(MnFe)Si dispersoids. When the samples reach the formation temperature of α-Al(MnFe)Si, for example above 573-648 K (350-375 ºC), α-Al(MnFe)Si dispersoids started to nucleate and grow along the $<001>_{Al}$ direction in the Si-rich sites of the previously metastable Mg_2Si (Fig. 12c). During heating process, two possible metastable phases could be formed under different heating rates, namely, β″-Mg_2Si and β′-Mg_2Si. The results obtained in the present work indicated that pre-existing β′-Mg_2Si

precipitates were more effective in the promotion of the dispersoid nucleation than pre-existing β”-Mg_2Si. This probably implies that the size of the lath-like β’-Mg_2Si precipitates was larger than that of needle-like β”-Mg_2Si, and thus the available Si on Si-rich sites of the former was higher than that of the latter, resulting in a more favorable condition for dispersoid nucleation and growth.

It is understandable that in the Mg-free base alloy, no pre-existing metastable Mg_2Si could be formed during the heating process. Thus, the precipitation of α-Al(MnFe)Si dispersoids was so difficult that only an insufficient number of dispersoids formed even after extensively prolonged heat treatment (648K(375ºC)/72h). It is obvious that Mg element is crucial for the precipitation of α-Al(MnFe)Si dispersoids because Mg promotes the formation of uniformly distributed Mg_2Si precipitates, which provide the nucleation sites for the α-Al(MnFe)Si dispersoids when Mg_2Si precipitates were dissolved during heat treatment. In previous works [17, 18], the pre-existing β’-Mg_2Si was reported to be the prerequisite for a high density nucleation of α-Al(MnFe)Si dispersoids in Mn containing Al-Mg-Si alloys, which is confirmed by the present work in the Al-Mn-Mg 3xxx alloy.

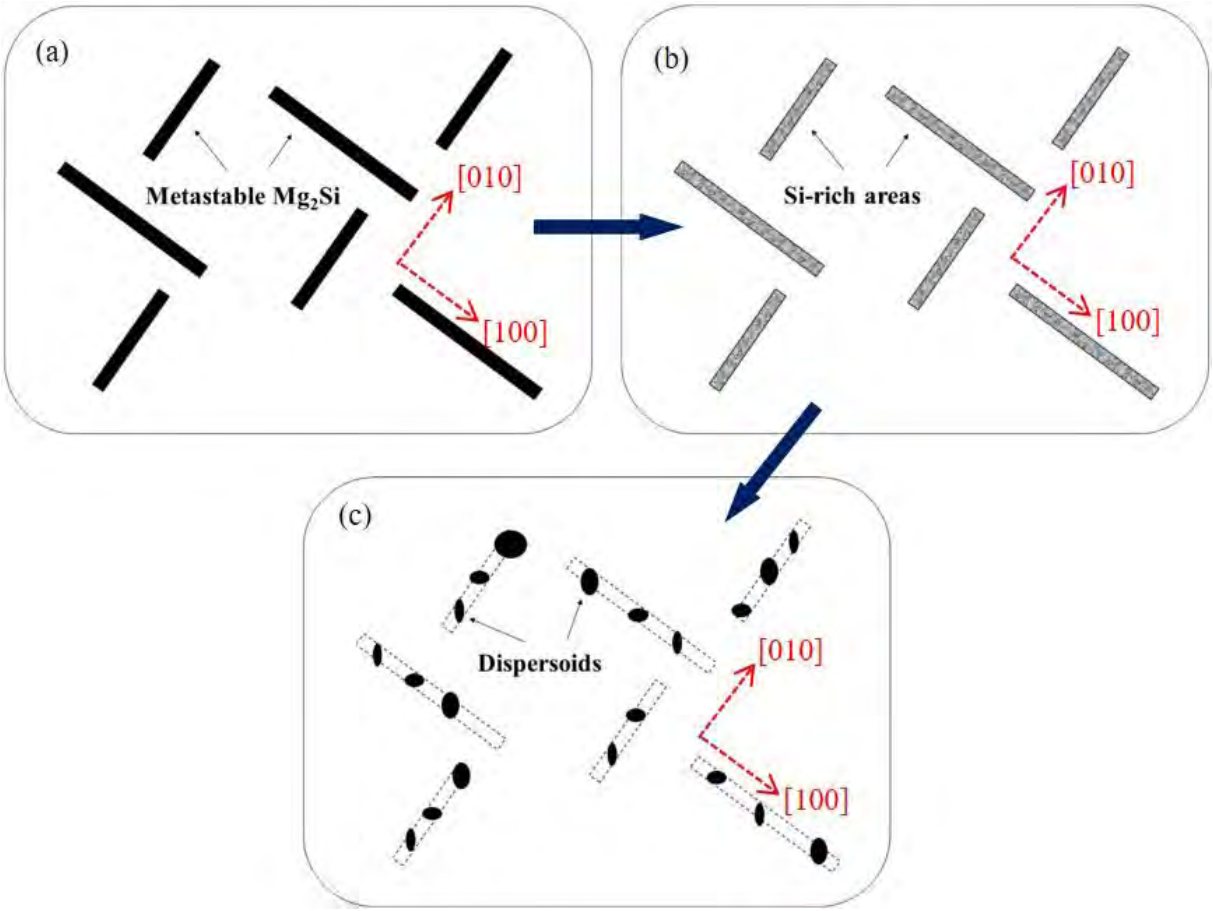

Fig. 12 Schematic diagram of the dispersoid formation based on metastable Mg_2Si nucleation mechanism, (a) metastable Mg_2Si precipitated, (b) Mg_2Si dissolved forming Si-rich areas and (c) α-Al(MnFe)Si disperspoid nucleation and growth in the Si-rich sites of previous metastable Mg_2Si along the $<001>_{Al}$ direction.

3.6 Dislocation-based nucleation mechanism

As described in Section 3.3, the cold deformation of the M1 sample that generated a great number of dislocations had an important influence on the dispersoid precipitation. {111} planes are the close-packed planes of aluminum and they are also the main dislocation slip planes. Hence, TEM bright field images were taken on the (-111) plane near the [011] zone axis to observe the dislocations and the precipitation process (see Fig. 13). After the deformed sample was heated to 548 K (275 ºC), both β'-Mg_2Si and dislocations can be observed as shown in Fig. 13a and b. When the deformed M1 sample held at 648 K (375 ºC) for 1 h, dispersoids and dislocations coexisted in aluminum matrix, but the β'-Mg_2Si disappeared and dissolved (Fig.

13c). Here, most of the dispersoids precipitated on dislocations, markedly different from the precipitation seen in the non-deformed sample (Fig. 9a).

To verify the orientation relationship between the α-Al(MnFe)Si dispersoids and the β'-Mg_2Si precipitates, the microstructure of the deformed samples was observed with the (200) crystal plane near the [001] direction. Growing along the $<001>_{Al}$ direction, lath-like β'-Mg_2Si precipitates were clearly seen without any interference from the dislocations in the sample heated to 548 K (275 ºC) (Fig. 13b). The sample held at 648 K (375 ºC) for 1 h showed that β'-Mg_2Si had already dissolved but that α-Al(MnFe)Si dispersoids did not lie along the $<001>_{Al}$ direction, but rather along the dislocations (Figs. 13c and d). This finding indicates that the sites of the previous β'-Mg_2Si precipitates were no longer the priority locations for dispersoids nucleation in the deformed sample. Due to the presence of a great number of dislocations, the fast diffusion of the alloying elements (including Si) would weaken the advantage of the local Si enrichment from the dissolved β'-Mg_2Si for α-Al(MnFe)Si dispersoid nucleation. Instead of the sites of previous β'-Mg_2Si, dislocations become the predominate sites for the dispersoid nucleation in the deformed sample.

When the deformed sample was held for 24 hours at 648 K (375 ºC), the dispersoids kept growing and became coarse (Fig. 13e). The size of dispersoids in the deformed sample after heating at 648 K (375 ºC) for 24 h was larger than that in the non-deformed sample, whereas the number density of dispersoids in the former is less than that in the latter (Table 2). It is likely that the fast diffusion of alloying elements through the dislocations can benefit the Ostwald ripening of dispersoids (coarsening). However, the volume fraction of the dispersoids in the deformed sample remains at a level similar to that found in the non-deformed sample.

In the as-cast microstructure, there were Mn depletion zones close to the Al_6(Mn,Fe) intermetallic particles and to the aluminum grain boundaries [33], causing the DFZs during heat treatment because of the lack of the essential element Mn required for α-Al(MnFe)Si dipersoid formation (Fig. 4). In the deformed sample, a great number density of dislocation piled up around intermetallic particles and grain boundaries because the intermetallic particles and grain boundaries were barriers to block dislocation migrations during deformation. During heat treatment, these dislocations acted not only as fast diffusion channels to transport Mn solutes to the Mn depletion zones but also as favorable nucleation sites, making the nucleation and growth of α-Al(MnFe)Si dipersoids possible in those zones. This is why, besides the dense dispersoid

zones in the cores of the aluminum grains, there were the less dense despersoid zones close to the $Al_6(Mn,Fe)$ intermetallic particles and grain boundaries in the deformed sample (Fig. 6), which was the DFZ where the precipitation of α-Al(MnFe)Si was impossible in the non-deformed sample. This resulted in a large reduction of DFZs and a more uniform dispersoid distribution when compared to the non-deformed sample.

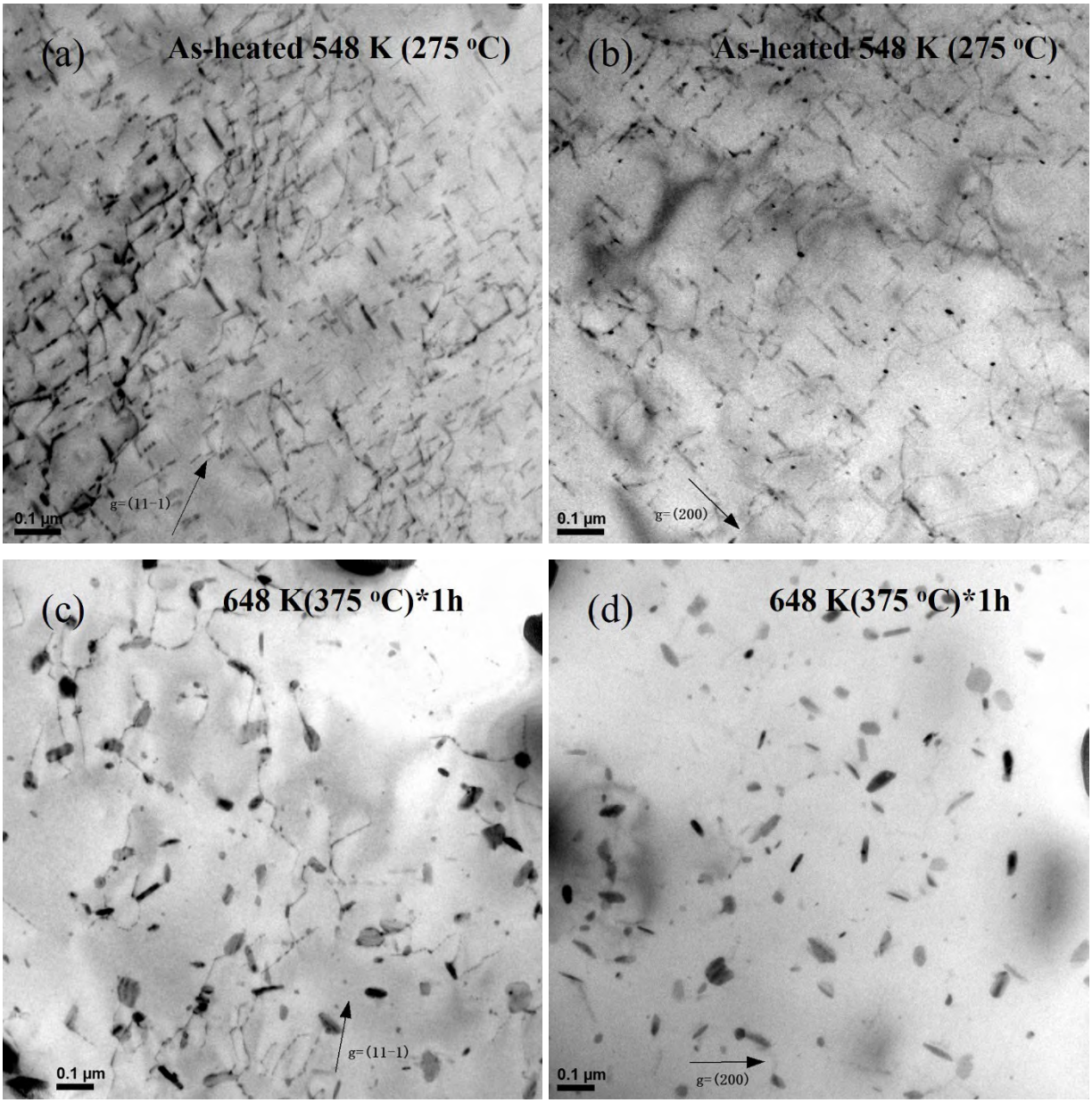

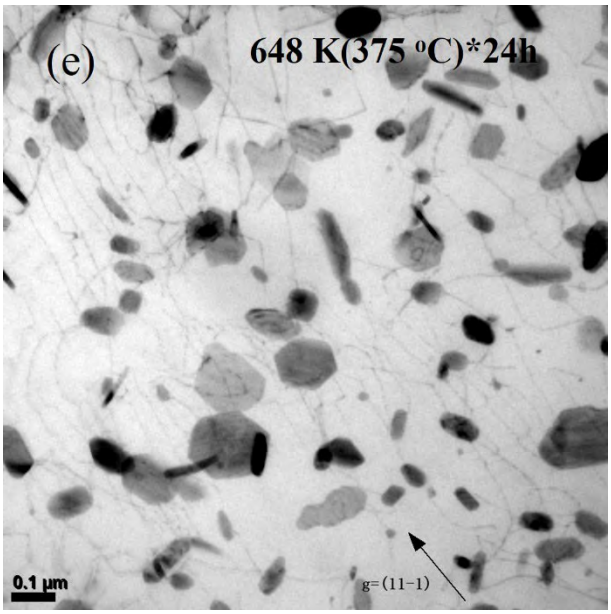

Fig. 13 The precipitation process in the deformed M1 samples (a) heated to 548 K (275 ºC) showing dislocations, recorded near $[011]_{Al}$; (b) heated to 548 K (275 ºC) showing β'-Mg_2Si, recorded near $[001]_{Al}$; (c) held at 648 K (375 ºC) for 1 h, recorded near $[011]_{Al}$, (d) held at 648 K (375 ºC) for 1 h, recorded near $[001]_{Al}$; (e) held at 648 K (375 ºC) for 24 h, recorded near $[011]_{Al}$.

Based on the above results, the nucleation mechanism of the dispersoids based on dislocations in the deformed sample can be schematically expressed as follows (Fig. 14). During the heating process toward 548 K (275 ºC), metastable β'-Mg_2Si phase first precipitated out, and a great number of dislocations and β'-Mg_2Si co-existed in the microstructure (Fig. 14a). As the temperature continued to increase toward 648 K (375 ºC), β'-Mg_2Si precipitates dissolved before the precipitation of α-Al(MnFe)Si dispersoids, and many dislocations remained in the aluminum matrix (Fig. 14b). Although the effect of local Si enrichment became weaker due to the fast diffusion of Si along dislocations, Si-rich areas would still exist in the aluminum matrix. When the temperature rose above the precipitation temperature of the dispersoids (thermal holding at 648 k (375 ºC)), α-Al(MnFe)Si dispersoids began to nucleate and grow on the dislocations and Si-rich areas (Fig. 14c). Generally, the size of the dispersoids nucleated on dislocations was larger than that on Si-rich areas due to the fast diffusion of atoms though dislocations (see Fig.13e). In the deformed sample, the dislocations acted as the preferable sites for the dispersoid

nucleation. Due to the fast diffusion of the alloying elements and favorable nucleation conditions created by the presence of a great number of dislocations, α-Al(MnFe)Si dispersoids can also precipitate in the Mn depleted zone (formerly the DFZ) close to intermetallic particles and grain boundaries, resulting in an overall uniform dispersoid distribution by reducing the DFZs in the microstructure.

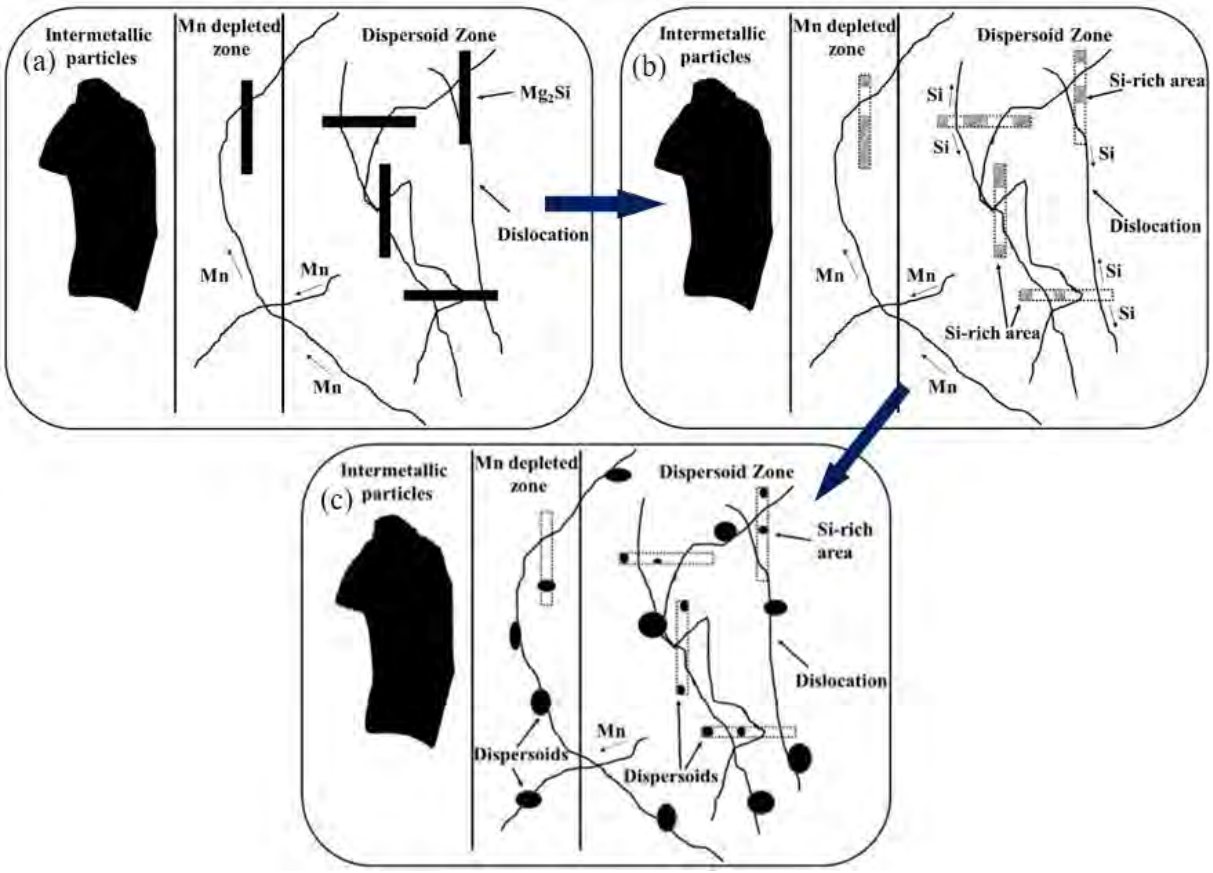

Fig. 14 Schematic diagram of the dislocation-based nucleation mechanism of α-Al(MnFe)Si dispersoids in the deformed sample, (a) metastable Mg_2Si precipitated and co-existed with dislocations; (b) metastable Mg_2Si dissolution and Si and Mn diffusion along dislocations and (c) α-Al(MnFe)Si dispersoid nucleation and growth on dislocations including in the Mn depleted zone (formerly the DFZ).

5. Conclusions

1) In Al-Mn-Mg 3xxx alloys, Mg plays an important role in promoting the formation of α-Al(MnFe)Si dispersoids. Without Mg addition, the precipitation of α-Al(MnFe)Si

dispersoids was so difficult that only an insufficient number of dispersoids could be obtained. The number density and volume fraction of the dispersoids in the Mg containing alloy are much higher than that in the base alloy without Mg, resulting in a strong dispersoid strengthening effect.

2) During heating process of the heat treatment of the Mg containing alloy, metastable Mg_2Si precipitated and dissolved, leaving local Si-rich areas, which provided favorable nucleation sites for α-Al(MnFe)Si dispersoids. Both metastable β''-Mg_2Si and β'-Mg_2Si have a positive effect on increasing the number density and volume fraction of the dispersoids. However, equilibrium β-Mg_2Si precipitates do not have any effect on the dispersoid formation.

3) β'-Mg_2Si precipitates are more effective than β''-Mg_2Si in promoting dispersoid nucleation. It could be attributed to the fact that β'-Mg_2Si would provide more available Si in the Si-rich areas for α-Al(MnFe)Si nucleation and growth than β''-Mg_2Si.

4) In the deformed sample, the dislocations become the preferable sites for α-Al(MnFe)Si dispersoid nucleation. Due to the presence of a great number of dislocations, α-Al(MnFe)Si dispersoids can nucleate and grow in the Mn depleted zone (formerly the DFZ) close to intermetallic particles and grain boundaries, resulting in a more uniform dispersoid distribution compared to the non-deformed sample.

5) The dispersoid nucleation mechanisms based on both metastable Mg_2Si and dislocations are proposed and discussed.

Acknowledgments

The authors would like to acknowledge the financial support of the Natural Sciences and Engineering Research Council of Canada (NSERC) and Rio Tinto Aluminum through the NSERC Industry Research Chair in the Metallurgy of Aluminum Transformation at University of Quebec at Chicoutimi.

References

1. K. Liu and X. G. Chen: *Mater. Design,* 2015, vol. 84, pp. 340-50.
2. Z. Li, Z. Zhang and X. G. Chen: *T. Nonferr. Metal. SOC.,* 2016, vol. 26, pp. 2793-99.
3. K. Liu and X.-G. Chen: *Metall. Trans. B,* 2016, vol. 47, pp. 3291-300.
4. Y. J. Li, A. M. F. Muggerud, A. Olsen and T. Furu: *Acta Mater.,* 2012, vol. 60, pp. 1004-14.
5. A. M. F. Muggerud, E. A. Mørtsell, Y. Li and R. Holmestad: *Mat. Sci. Eng. A,* 2013, vol. 567, pp. 21-8.
6. Y. J. Li and L. Arnberg: *Acta Mater.,* 2003, vol. 51, pp. 3415-28.
7. A. M. F. Muggerud, J. C. Walmsley, R. Holmestad and Y. Li: *Philos. Mag.,* 2015, vol. 95, pp. 744-58.
8. K. Liu, H. Ma and X. G. Chen: *J. Alloy. Compd.,* 2017, vol. 694, pp. 354-65.
9. G. A. Edwards, K. Stiller, G. L. Dunlop and M. J. Couper: *Acta Mater.,* 1998, vol. 46, pp. 3893-904.
10. C. D. Marioara, S. J. Andersen, H. W. Zandbergen and R. Holmestad: *Metall. Trans. A,* 2005, vol. 36, pp. 691-702.
11. S. J. Andersen, H. W. Zandbergen, J. Jansen, C. TrÆholt, U. Tundal and O. Reiso: *Acta Mater.,* 1998, vol. 46, pp. 3283-98.
12. R. Vissers, M. A. van Huis, J. Jansen, H. W. Zandbergen, C. D. Marioara and S. J. Andersen: *Acta Mater.,* 2007, vol. 55, pp. 3815-23.
13. M. Murayama and K. Hono: *Acta Mater.,* 1999, vol. 47, pp. 1537-48.
14. C. S. Tsao, C. Y. Chen, U. S. Jeng and T. Y. Kuo: *Acta Mater.,* 2006, vol. 54, pp. 4621-31.
15. M. H. Jacobs: *Philos. Mag.,* 1972, vol. 26, pp. 1-13.
16. X. Wang, S. Esmaeili and D. J. Lloyd: *Metall Trans. A,* 2006, vol. 37, pp. 2691-99.
17. H. Hirasawa: *Scripta Mater.,* 1975, vol. 9, pp. 955-8.
18. L. Lodgaard and N. Ryum: *Mat. Sci. Eng. A,* 2000, vol. 283, pp. 144-52.
19. R. Hu, T. Ogura, H. Tezuka, T. Sato and Q. Liu: *J. Mat. Sci. Tec.,* 2010, vol. 26, pp. 237-243.
20. Z. Li, Z. Zhang and X. G. Chen: *Metals,* 2018, vol. 8, pp. 155.
21. C. Genevois, D. Fabrègue, A. Deschamps and W. J. Poole: *Mat. Sci. Eng. A,* 2006, vol. 441, pp. 39-48.
22. A. Deschamps, F. Livet and Y. Bréchet: *Acta Mater.,* 1998, vol. 47, pp. 281-92.
23. A. Deschamps and Y. Brechet: *Acta Mater.,* 1998, vol. 47, pp. 293-305.
24. R. S. Yassar, D. P. Field and H. Weiland: *Scripta Mater.,* 2005, vol. 53, pp. 299-303.
25. D. Yin, Q. Xiao, Y. Chen, H. Liu, D. Yi, B. Wang and S. Pan: *Mater. Design,* 2016, vol. 95, pp. 329-39.
26. T. Saito, S. Muraishi, C. D. Marioara, S. J. Andersen, J. Røyset and R. Holmestad:

Metall. Trans. A, 2013, vol. 44, pp. 4124-35.
27. S. P. Chen, N. C. W. Kuijpers and S. van der Zwaag: *Mater. Sci. Eng. A*, 2003, vol. 341, pp. 296-306.
28. J. D. Robson, T. Hill and N. Kamp: *Mater. Sci. Forum*, 2014, vol. 794, pp. 697-703.
29. Z. Li, Z. Zhang, X. G. Chen: *Mater. Sci. Eng. A*, 2017, vol. 708, pp. 383-394
30. D. Tabor: *J. I. Met.*, 1951, vol. 79, pp. 1-18.
31. W. Yang, M. Wang, X. Sheng, Q. Zhang, L. Huang: *Philosophical Magazine Letters*, 2011, vol. 91, pp. 150-160
32. W. Yang, M. Wang, R. Zhang, Q. Zhang, X. Sheng: *Scripta Mater.*, 2010, vol. 62, pp. 705-708
33. Q. Du, W. J. Poole, M. A. Wells and N. C. Parson: *Acta Mater.*, 2013, vol. 61, pp. 4961-73.

Tables

Table 1 Chemical composition of experimental alloys (wt%)

Alloy code	Si	Fe	Mn	Mg	Al
Base	0.23	0.56	1.23	**0.002**	Bal.
M1	0.26	0.57	1.25	**1.00**	Bal.

Table 2 Dispersoid and DFZ parameters measured under different conditions

Alloy	Heat treatment	Area fraction of DFZ (%)	Equivalent diameter of dispersoids (nm)	Number density of dispersoids (μm^{-3})	Volume fraction of dispersoids (%)
Base	648K(375ºC)/24h	79	97	72	0.32
Base	648K(375ºC)/24h	51.4	80	-	0.82
M1 Alloy	648K(375ºC)/24h	26.4	50	1055	2.69
M1 Alloy	448K(175ºC)/5h + 648K(375ºC)/24h	30	56	563	1.93
M1 Alloy	523K(250ºC)/12h + 648K(375ºC)/24h	23	42	1326	2.15
Deformed M1 Alloy	648K(375ºC)/24h	7	68	294	2.58

A List of Figure Captions

Fig. 1 Schematic diagram of various heat treatments (a) procedure A and (b) procedure B (two-step heat treatment).

Fig. 2 Optical images showing the dispersoid distribution in the base alloy, (a) 648 K (375 °C) for 24 h and (b) 648 K (375 °C) for 72 h.

Fig. 3 TEM bright field images showing the dispersoids in the base alloy, (a) 648 K (375 °C) for 24 h and (b) 648 K (375 °C) for 72 h, recorded near $[001]_{Al}$ zone axis.

Fig. 4 Optical images showing the precipitation of dispersoids in the M1 alloy under different heat treatment conditions, (a) 648K(375ºC)/24h, (b) 448K(175ºC)/5h + 648K(375ºC)/24h and (c) 523K(250ºC)/12h + 648K(375ºC)/24h.

Fig. 5 TEM bright field images showing the dispersoids in the M1 alloy after different heat treatments, (a) 648K(375ºC)/24h, (b) 448K(175ºC)/5h + 648K(375ºC)/24h and (c) 523K(250ºC)/12h + 648K(375ºC)/24h, recorded near the $[001]_{Al}$ zone axis. The arrows indicate the $<100>_{Al}$ orientation.

Fig. 6 Optical image showing the precipitation of dispersoids in the deformed M1 alloy after heat treatment at 648K(375ºC)/24h: (a) the dense dispersoid zone and the less dense dispersoid zone and (b) enlarged image of (a).

Fig. 7 TEM bright field images showing the dispersoids in the deformed M1 alloy (0.2 strain + 648K(375ºC)/24h), a) in the dense dispersoid zone and b) in the less dense dispersoid zone.

Fig. 8 Microhardness of the base alloy and M1 alloy under various experimental conditions.

Fig. 9 The precipitation process in the M1 alloy (a) as-heated at 548 K (275 ºC), (b) as-heated at 648 K (375 ºC), (c) 648 K (375 ºC) for 30 min, (d) 648 K (375 ºC) for 1 h, (e) 648 K (375 ºC) for

2 h, (f) the selected area diffraction pattern (SADP) corresponding to the image (a) and the typical diffraction spots of β′-Mg_2Si indicated by the red circles.

Fig. 10 TEM analysis of the M1 sample held at 648 K (375 ºC) for 15 minutes showing the local Si enrichment on the sites of previous β′-Mg_2Si precipitates, (a) TEM image on the site of a previous β′-Mg_2Si and the position of the line scanning (A-C) and (b) Si distribution along the line A-C.

Fig. 11 TEM images of the M1 samples experienced (a) 448 K (175 ºC) for 5 h, (b) 523 K (250 ºC) for 12 h, (c) 448 K (175 ºC) for 5 h + 648 K (375 ºC) for 1 h, (d) 523 K (250 ºC) for 12 h + 648 K (375 ºC) for 1 h, (e) the selected area diffraction pattern (SADP) corresponding to the image (a) and the typical diffraction spots of β″- Mg2Si indicated by the red circles, (f) the selected area diffraction pattern (SADP) corresponding to the image (b) and the typical diffraction spots of β′-Mg_2Si indicated by the red circles.

Fig. 12 Schematic diagram of the dispersoid formation based on metastable Mg_2Si nucleation mechanism, (a) metastable Mg_2Si precipitated, (b) Mg_2Si dissolved forming Si-rich areas and (c) α-Al(MnFe)Si disperspoid nucleation and growth in the Si-rich sites of previous metastable Mg_2Si along the $<001>_{Al}$ direction.

Fig. 13 The precipitation process in the deformed M1 samples (a) heated to 548 K (275 ºC) showing dislocations, recorded near $[011]_{Al}$; (b) heated to 548 K (275 ºC) showing β′-Mg_2Si, recorded near $[001]_{Al}$; (c) held at 648 K (375 ºC) for 1 h, recorded near $[011]_{Al}$, (d) held at 648 K (375 ºC) for 1 h, recorded near $[001]_{Al}$; (e) held at 648 K (375 ºC) for 24 h, recorded near $[011]_{Al}$.

Fig. 14 Schematic diagram of the dislocation-based nucleation mechanism of α-Al(MnFe)Si dispersoids in the deformed sample, (a) metastable Mg_2Si precipitated and co-existed with dislocations; (b) metastable Mg_2Si dissolution and Si and Mn diffusion along dislocations and (c) α-Al(MnFe)Si dispersoid nucleation and growth on dislocations including in the Mn depleted zone (formerly the DFZ).